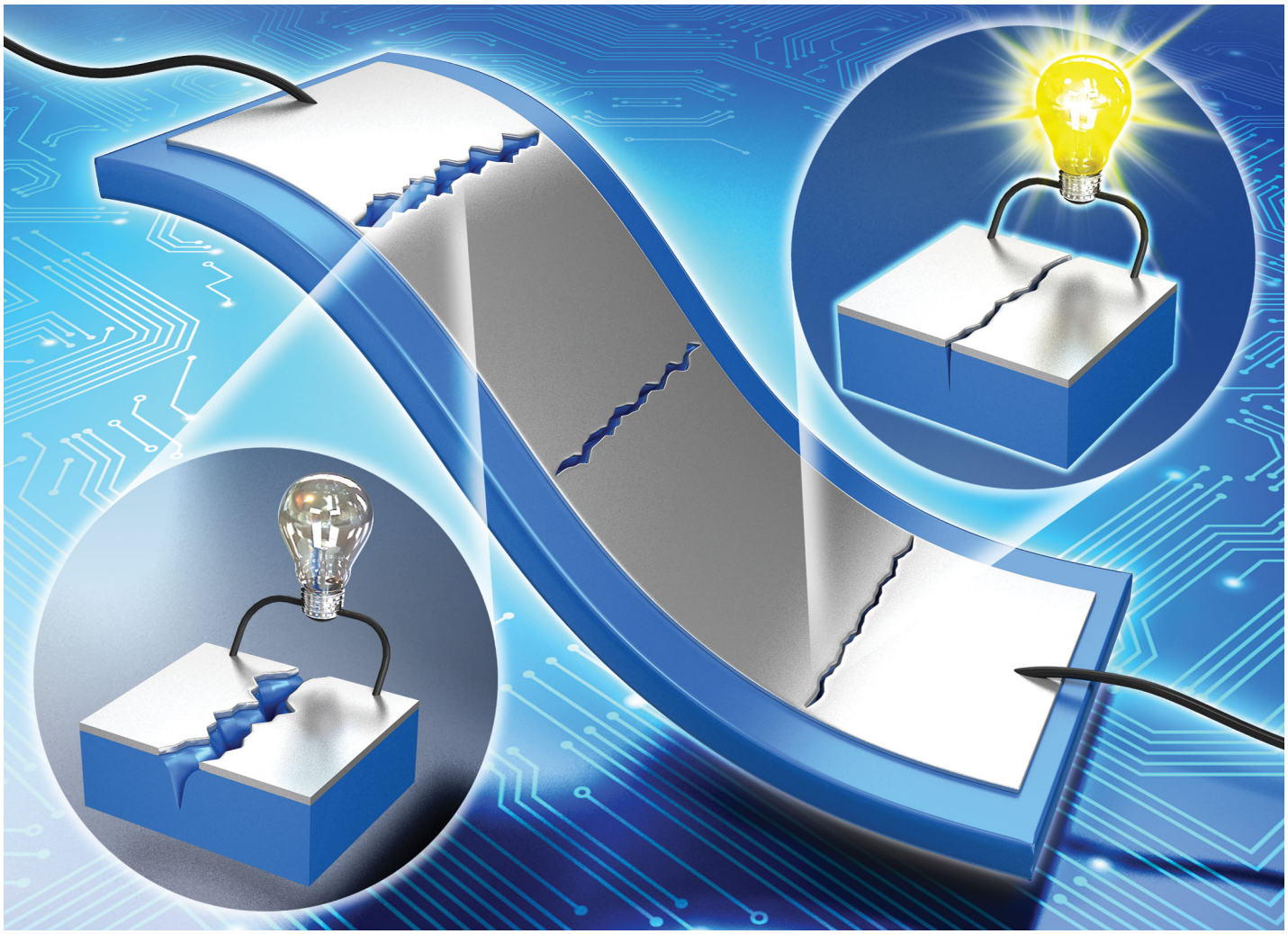

Showcasing research from the Global Frontier Center for Multiscale Energy Systems, Seoul National University.

Metal–elastomer bilayered switches by utilizing the superexponential behavior of crack widening

We developed a metal–elastomer bilayer switch utilizing super exponential behavior of crack widening. Super exponential behavior of a crack leads to infinite resistance while the 2% strain is applied.

As featured in:

See Sang Moon Kim, Daeshik Kang, Mansoo Choi *et al.*, *J. Mater. Chem. C*, 2017, **5**, 10920.

ROYAL SOCIETY OF CHEMISTRY

rsc.li/materials-c

Registered charity number: 207890

Journal of Materials Chemistry C

COMMUNICATION

View Article Online
View Journal | View Issue

Cite this: J. Mater. Chem. C, 2017, 5, 10920

Received 13th June 2017,
Accepted 15th September 2017

DOI: 10.1039/c7tc02630g

rsc.li/materials-c

Metal–elastomer bilayered switches by utilizing the superexponential behavior of crack widening†

Gunhee Lee,‡[ab] Taemin Lee,‡[ab] Yong Whan Choi,‡[a] Peter V. Pikhitsa,[a] Sei Jin Park,[a] Sang Moon Kim,*[c] Daeshik Kang *[d] and Mansoo Choi*[ab]

Strain gated switch systems have recently been developed for direct human–machine interfacing wearable electronics. These switch systems that use piezotronic nanowires or metal/elastomer bilayer films have limitations of low on–off ratios or large threshold strain. Herein, we present a metal–elastomer bilayer reversible switch system utilizing the superexponential behavior of crack widening. The crack width exhibits a superexponential dependence on the applied strain, instead of a linear dependence of regular widening. Such superexponential behavior of widening of a crack leads to an almost infinite resistance of the metal film when the applied strain approaches 2%. The resistance of the switch increases approximately by 5 orders of magnitude when 1.6% strain is applied, resulting in an overall gauge factor that exceeds 6 × 10^6, which shows that our device can perform as a switch. By combination of metal–elastomer bilayer strain-gated switches, we demonstrated logic elements such as AND, OR, NAND, and NOR gates by expressing the gestures of fingers as numbers on a seven-segment display. The newly proposed switch system also showed excellent durability, reproducibility, low energy consumption and tunable threshold strain.

1. Introduction

Wearable electronics is a rapidly emerging research field because it integrates technology into human daily lives, and has potential applications in various areas such as human–machine interfacing,[1–4] ubiquitous computing,[5,6] and healthcare.[7–10] In order to operate these devices, signal acquisition and processing are essential, and among various mechanical stimuli that can be sensed, stretching of the skin is one of the most readily available information. This strain may arise from voluntary movements of joints and muscles, or autonomic functions such as heartbeats and respiration, which can then be converted into electrical signals for processing. To date, various flexible strain sensors have been developed, including those based on nanowires,[11–13] graphenes,[14–16] carbon nanotubes,[17–19] and other materials.[20–22] However, these sensors require a signal processing circuit which would introduce complexities in device design. Instead of producing an analog signal and then processing it, a simple strain-gated digital signal would be more appropriate for certain wearable applications such as motion capturing devices.[22] Strain gated logic devices such as switches or transistors have been developed by using piezotronic nanowires[23–26] and metal/elastomer bilayer films.[27] Of these devices, piezotronic nanowire switches have been designed to have a low threshold strain (~1%), but their on–off ratios are low ($I_{on}/I_{off} \leq 95.7$).[24] Metal–elastomer bilayer switches have a high on–off ratio, but operate in the compressive strain regime and their threshold strain was relatively large ($\varepsilon \geq 20\%$).[25] A switch that combines a high on–off ratio with low energy consumption and small threshold strain for detecting a tiny movement of the skin has yet to be demonstrated (Fig. S1, ESI†).

Previously, Kang *et al.*[28] reported a fractured metal thin film/elastomer bilayer strain sensor with a platinum/polyurethane acrylate (PUA) stack. In the present work, we found that by changing the crack widening behavior on the elastomer substrate, the resistance change becomes more sensitive to the applied strain, and hence we used the device as a strain gated switch instead of a strain sensor. To achieve this purpose, we replaced PUA with a highly stretchable (~200% strain) and soft (elastic modulus ~5 MPa) silicone rubber as a substrate. Unlike a platinum/PUA stack, the conduction pathway of the platinum/silicone rubber stack is completely broken at only over 2% strain. Using this strain-gated switch, we fabricated logic elements such as AND, OR, NAND, and NOR gates and

[a] Global Frontier Center for Multiscale Energy Systems, Department of Mechanical and Aerospace Engineering, Seoul National University, Seoul 151-742, Korea. E-mail: mchoi@snu.ac.kr
[b] Division of WCU Multiscale Mechanical Design, Department of Mechanical and Aerospace Engineering, Seoul National University, Seoul 151-742, Korea
[c] Department of Mechanical Engineering, Incheon National University, Incheon, 406-772, Korea. E-mail: ksm7852@inu.ac.kr
[d] Department of Mechanical Engineering, Ajou University, San 5, Woncheon-dong, Yeongtong-gu, Suwon 443-749, Republic of Korea. E-mail: dskang@ajou.ac.kr
† Electronic supplementary information (ESI) available. See DOI: 10.1039/c7tc02630g
‡ These authors contributed equally to this work.

demonstrated a simple figure gesture induced complex electrical signaling.

2. Experimental

2.1. Preparation of a silicone rubber film

Polydimethylsiloxane (PDMS) (Dow Corning, Sylgard 184) was bonded on glass by oxygen plasma treatment (CUTE-1MPR, Femto Science Inc.). Silicone rubber compounds (KEG-2000-60A/B, Shin-Etus) were poured into a PDMS/glass mold. Then a glass cover was placed on the mixture, and a pressure of 2 MPa was applied at 140 °C on a hot plate. The silicone rubber was cured for 10 minutes, and subsequently the film was demolded.

2.2. Strain-gated switch fabrication

For curved switches, a silicone rubber film (250 μm thick) was stretched to 8% strain and another silicone rubber (250 μm thick) film was bonded to it by an oxygen plasma treatment for 40 seconds. For flat switches, a flat 500 μm thick silicone rubber film (5 × 15 mm^2) was used. For threshold strain-controllable switches, a silicone rubber film (250 μm thick) underlying the substrate was stretched (0, 5, 10, 15% strain) using a custom-built stretcher, and then bonded to another silicone rubber film (250 μm thick) layer in an area of 5 × 3 mm^2 by an oxygen plasma treatment. A 20 nm thick platinum layer was deposited on the elastomeric substrate using a sputter (Ultech Inc.). Then the stack was stretched by a custom-built stretcher in order to generate cracks (Fig. 4a and Fig. S2, S9, ESI†).

2.3. Testing of the strain-gated switch

The switch was clamped in an all-electric test instrument (3342 UTM, Instron Co.) and stretched by using specified maximum strain and force at 1 mm min^{-1}. The resistance change was measured using a LabView based PXI-4071 system (NI Instruments).

3. Results and discussion

Fig. 1a illustrates the operating principle of the strain-gated switch. Cracks are formed on the metal–elastomer bilayer due to the difference in the elastic modulus between the two layers, when the switch is stretched to 2% strain. When the device is stretched above a threshold, the crack opens up (Fig. 1a, top right), turning the switch 'off'. And when the device is compressed, the crack closes (Fig. 1a, bottom right), turning the switch 'on'. To confirm the operation of the switch, a simple circuit with a light emitting diode (LED) was used. When the switch stretched to over 2% strain, it is 'off', and the microscale cracks open up, which results in the turning off of the LED (Fig. 1b). When the switch is released, it is 'on', the microscale cracks close, and the LED turns on (Fig. 1c). The difference between the previously

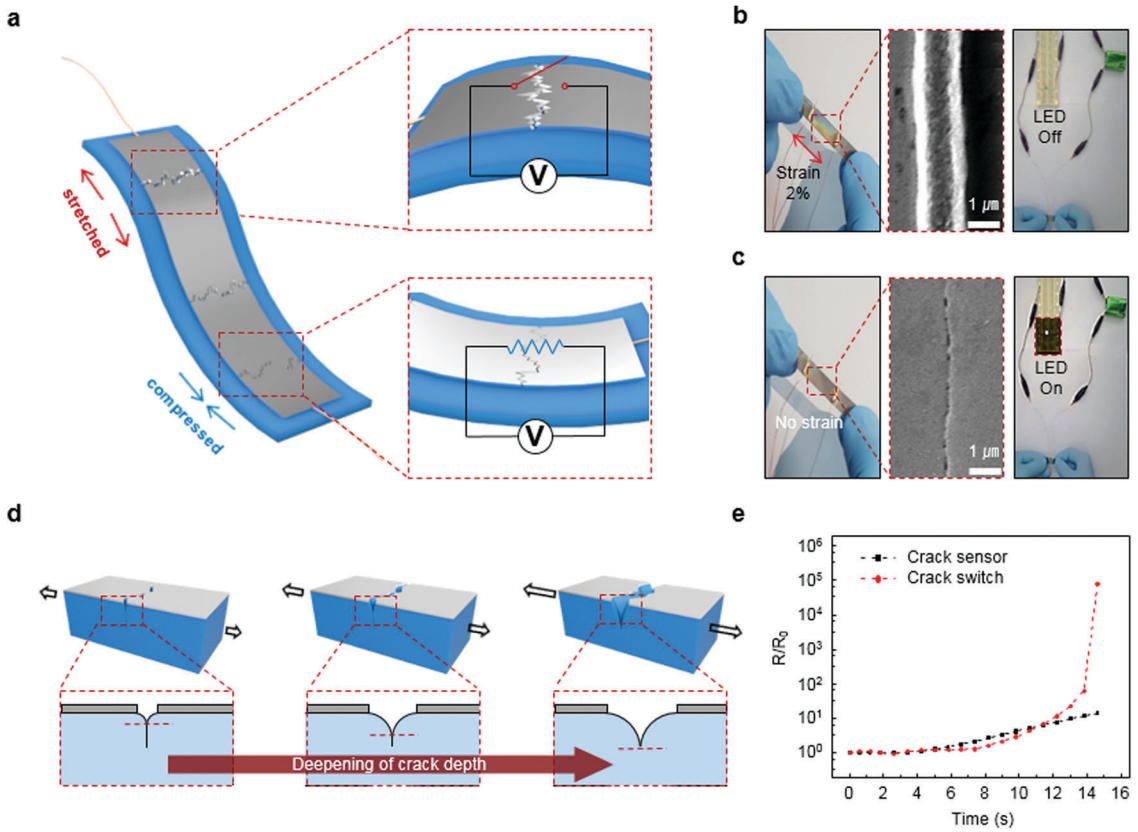

Fig. 1 (a) Schematic illustration of operating strain-gated switches. (b and c) Photo images for operating strain-gated switches and the corresponding SEM images of opened and closed cracks. (d) Schematic illustration of the superexponential behavior of crack widening with variation of strain. (e) Comparison of normalized resistance variance between the crack sensor and the crack switch when strain is applied to the devices.

reported crack-based sensor[28] and the current switch is as follows. By changing the substrate from the PUA film to the soft elastomeric material, the crack opening behavior is changed, and the use of silicone rubber results in a non-linear widening of the crack opening (Fig. 1d), as opposed to the linear opening that was seen in the previous sensor with the PUA substrate.[28] This then translates into totally different behavior in resistance increase. As the strain applied to the devices increases, the resistance of the switch increases dramatically, whereas the previous sensor showed a linear increase (Fig. 1e).

To study the switching mechanism, we measured the electrical resistance change of the metal film and the variation of geometrical features, such as crack depth and width, with the variation of applied strains. Fig. 2a shows the crack depth and width on the platinum/silicone rubber stack measured using atomic force microscopy (AFM) with the variation of strains. The results indicate that the crack depth increases as the applied strain increases, which leads to the superexponential behavior of the widening of the crack.

The resistance change during repeated stretching and relaxation of the switch is shown in Fig. 2b. When 1.6% strain is applied, the device resistance increases approximately by 5 orders of magnitude, and when relaxed, the resistance decreases to the nominal value of $\sim$30 Ω. The resistance is proportionally related to the crack width, and thus shows a superexponential dependence on the applied strain. The resistance change is strongly affected by the distance between crack lips because a wider crack gap means a fewer electrical contact points left. At 2% strain, the resistance of the device increases to infinity (at least 10^{12} Ω, Fig. 2b, inset) and the on–off ratio becomes $\sim 3 \times 10^{10}$, which is the limit of the measurement equipment. This probably means that the cracks are so widened that the conduction path through the islands of the crack metal layer is broken, and it does not contribute to conduction anymore. An optical microscopy image was taken to confirm that the conduction path through the metal islands is completely broken and the islands do indeed not touch each other (Fig. S3, ESI†). In addition, the crack switch can be used as a strain sensor as well, and the overall gauge factor determined from the definition $(\Delta R/R_0)/\varepsilon$ exceeds 6×10^6 over the 0 to 1.6% strain range as shown in Fig. 2b. It is noted that resistance variation to the applied strain is non-linear (the strain dependent gauge factor defined by the Gauge Factor = $(dR/R_0)/d\varepsilon$ is shown in Fig. S4 (ESI†)). The loading and unloading resistance changes are measured while subjecting the device to 1.6% strain in order to evaluate its hysteresis (Fig. 2c). The switch exhibits 0.1% hysteresis when measured using criteria used by Park and Yoon *et al.*,[29,30] which can be considered to be negligible. The response time to rapid stretching up to 0.4% strain is approximately 100 ms (Fig. 2d). This delay is presumably related to the viscoelasticity of

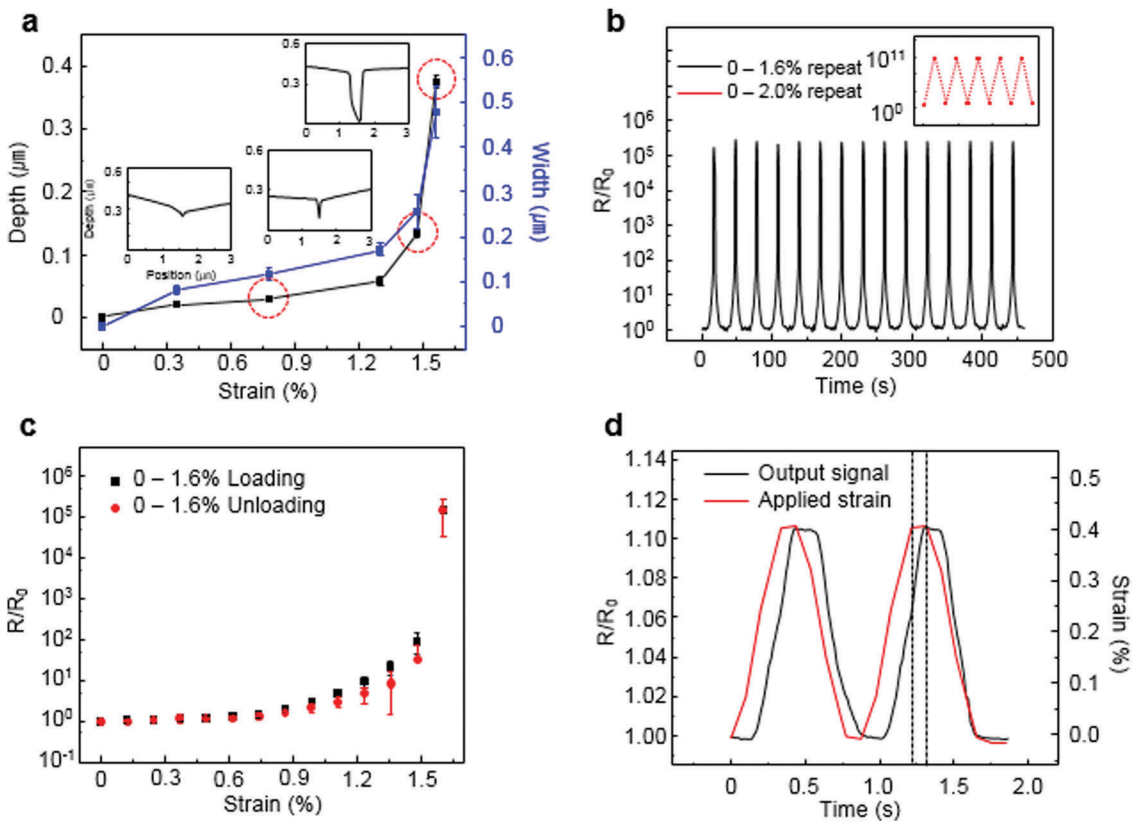

Fig. 2 (a) The variation of depth and width with the variation of applied strain. (b) The graph of normalized resistance variance *versus* a strain of 1.6% in 15 cyclic tests. (Inset: 2.0% in 5 cyclic tests). (c) The standard deviation and the average over 5 different samples in the hysteresis test of the strain gated switch. Red and black dots show unloading and loading states, respectively. (d) The response time of the strain gated switch. The red and black lines indicate the input signal (strain of 0.4%), and the response time of the input strain, respectively.

the soft polymeric substrate, which opens up further tuning opportunity of the substrate mechanics, and the device characteristics. The delay in response is on par with previous wearable devices such as wearable strain sensors and pressure sensors.[31,32] Furthermore, the durability of the switch was tested by cyclic loading and unloading, and the switch showed repeatable performance up to 5000 cycles (Fig. S5, ESI†).

For a simple demonstration of how strain-gated switches can be used in wearable devices, we constructed AND, OR, NAND and NOR gates by combinations of the switches. In the case of an AND gate, two switches are linearly connected, and the circuit is electrically connected only when the two switches are "on" (Fig. 3a). If the switches are mounted on different fingers which then are stretched, the input becomes "1,1", the circuit is electrically connected, and the LED turns on (Fig. 3b). In the case of an OR gate, two switches are connected in parallel as shown in Fig. 3c. In this case, only when the two fingers bent and the logic input becomes "0,0", the circuit is electrically disconnected and the LED turns off (Fig. 3d). AND and OR gates are built by using two open collector circuits shown in Fig. S6a and b (ESI†). When the switch is compressed, the device resistance ($\sim$30 Ω) is much lower than that of a pull-down resistor ($\sim$10 MΩ); hence the logic output is "1". When the switch is stretched and turns "off", the logic output becomes "0" as V_{out} is directly connected to ground (GND). Circuit diagrams for NAND and NOR gates are shown in Fig. 3e and g. In the case of a NAND gate, the LED is off when the two fingers are straight and input is "1,1" as shown in Fig. 3f. In the case of a NOR gate, the LED turns on when the two fingers are bent and the input becomes "0,0" (Fig. 3h). NAND and NOR gates are demonstrated with a totem pole crack switch circuit. By appropriate placement, the states of the switches can be designed to be opposite at all times by mounting them together with the metal layer on the opposing sides (Fig. S6c and d, ESI†). Depending on the motion of the joint, the combination of the switch states can lead to the logical output of either "1" or "0". Such strain gated logic devices can be used to provide more advanced responses from human skin movements.

As human skin can be stretched to various degrees according to movements of joints and muscles, the ability to manipulate the threshold strain of the switches is necessary for their integration in wearable devices. Fig. 4a illustrates the fabrication process of a curved switch whose critical radius of curvature is shifted. A silicone rubber (250 μm thickness) substrate is stretched to a strain of 8% and another silicone rubber (250 μm thickness) substrate is bonded by O_2 plasma treatment for 40 seconds. After releasing the two layered substrate, a thin Pt layer (20 nm) is deposited. The metal deposited substrate is then bent to a radius of 12.5 mm for crack generation on the epilayer. Fig. 4b illustrates a conceptual depiction of a curved switch which needs to unfold before the cracks can start widening. Therefore, curved switches would have shifted threshold strains, depending on their radii of curvature. By mounting two switches with different threshold strains on a single finger, the output level controlled by the degree of finger joint flexion can become "0,1", "1,1" or "1,0", under fully flexed, semi-flexed, and fully extended conditions, respectively (Fig. 4c). The switches and their combinations can be further integrated into a hand-worn device where finger-gestures can be translated into single decimal numerals on a seven-segment display, without requiring additional signal processing circuits. In order to create 7 distinct input signals with 5 fingers, 2 additional switches with shifted threshold strains were fabricated and attached to two fingers. Photographs of the seven-segment display that indicates the movement of five fingers are shown in Fig. 4d and e. The thumb and the ring finger bend and the output logic signal becomes "0", the middle finger is fully stretched and the output logic signal becomes "1,0", the index finger is semi-flex and the output logic signal becomes "1,1" and the little finger is fully stretched and the output logic signal becomes "1". Integrating each switch with each segment, number "7" is presented on the panel as shown in Fig. 4d. Meanwhile, the fully

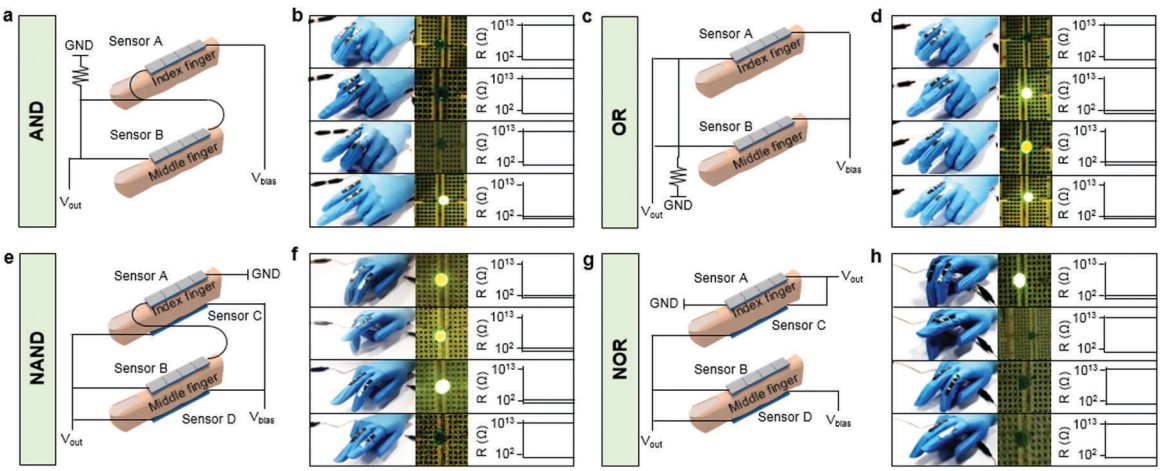

Fig. 3 Four logic gates with strain gated switches. (a, c, e and g) Schematic illustrations of AND (a), OR (c), NAND (e), and NOR (g) logic gates. Depending on the motion of the joint, the combination of the switch states led to logical output of either "1" or "0". (b, d, f and h) Demonstrations of LED "on/off" with respect to the corresponding logical output. The measured electrical output resistances of AND, OR, NAND, and NOR gates *versus* the mechanical input strains by the motion of the joint.

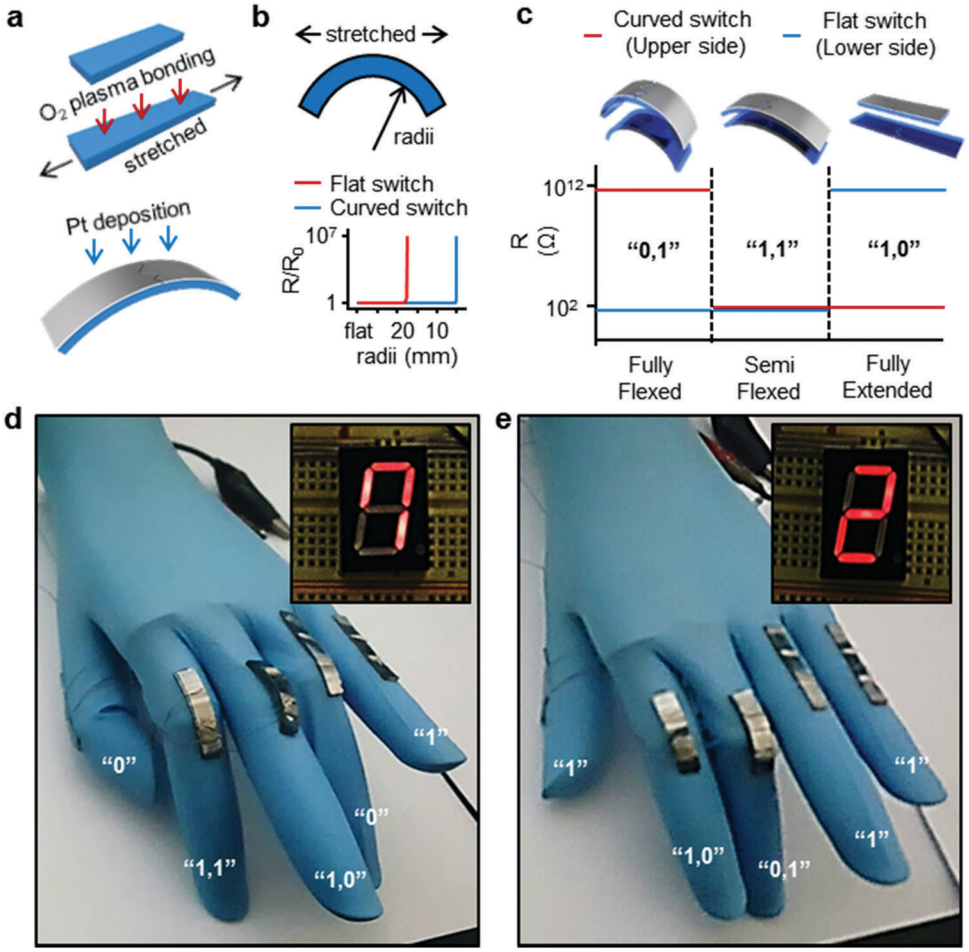

Fig. 4 (a) Schematic illustration of fabrication of a curved switch. (b) Shift of the threshold strain of the curved switch due to the predefined shape. (c) Resistance variance of the combination of the curved switch (upper side) and flat switch (lower side). Three output levels were created by mounting two switches with varied motions of the joints on fingers. (d and e) Photographs of output logic signals, "7" (d) and "2" (e), that appeared on the seven-segment display in accordance with varied motions of the five fingers.

stretched thumb, index finger, ring finger and little finger, and the fully flexed middle finger present number "2" (Fig. 4e). Details of signals expressed by fingers with the switch system and all the numbers (0–9) presented by using the seven-segment display are shown in Fig. S7 (ESI†).

In addition to shifting the critical radii of curvature, changing the threshold strain is shown in Fig. S8 (ESI†). For utilization of these switches in wearable devices on various body parts with applicable strain ranges such as the neck (<0.5%), face (<2%) and hand (<20%), the ability to manipulate the threshold strain of flat devices is required.[33] The range of threshold strains that can be achieved is 2 to 20%.

4. Conclusion

We have demonstrated a strain-gated, crack-based switch that takes advantage of the superexponential behavior of crack widening under tensile strain. The switch exhibits an ultrahigh on–off ratio and low threshold strain that are required for low energy consumption and detection of small strains. We have developed a theoretical model to predict the resistance change of the device depending on the crack widening, and showed that the predictions are consistent with the experiments. Logic gates (AND, OR, NAND, NOR) have been constructed by using multiple switches and appropriate circuit design, and finger-gesture translation into individual numbers on a seven-segment display has been demonstrated. The switch presented in this paper exhibits excellent reliability, low energy consumption, and tunable threshold strain, which make it an attractive candidate for integration into various wearable devices.

Conflicts of interest

There are no conflicts to declare.

Acknowledgements

G. Lee, Y. W. Choi, and T. Lee contributed equally to this work. M. Choi acknowledges financial support from the Global Frontier R&D Program of the Center for Multiscale Energy Systems (No. 2012M3A6A7054855) funded by the National Research Foundation (NRF) of Korea. D. Kang and S. M. Kim

acknowledge financial support from the Basic Science Research Program through the National Research Foundation of Korea (NRF) funded by the Ministry of Science, ICT & Future Planning (2016R1C1B1009689 and 2016R1C1B1014564). D. Kang and S. M. Kim acknowledge financial support from the new faculty research fund of Ajou University and the Ajou University research fund. This research was also supported by the Nano Material Technology Development Program through the National Research Foundation of Korea (NRF) funded by the Ministry of Science, ICT and Future Planning (2009-0082580).

References

1 W. Wu, X. Wen and Z. L. Wang, *Science*, 2013, **340**, 952–957.
2 E. Roh, B.-U. Hwang, D. Kim, B.-Y. Kim and N.-E. Lee, *ACS Nano*, 2015, **9**, 6252–6261.
3 S. Lim, D. Son, J. Kim, Y. B. Lee, J. K. Song, S. Choi, D. J. Lee, J. H. Kim, M. Lee and T. Hyeon, *Adv. Funct. Mater.*, 2015, **25**, 375–383.
4 J. Lee, H. Kwon, J. Seo, S. Shin, J. H. Koo, C. Pang, S. Son, J. H. Kim, Y. H. Jang and D. E. Kim, *Adv. Mater.*, 2015, **27**, 2433–2439.
5 P. Bonato, *IEEE Eng. Med. Biol. Mag.*, 2010, **29**, 25–36.
6 K. Jost, D. Stenger, C. R. Perez, J. K. McDonough, K. Lian, Y. Gogotsi and G. Dion, *Energy Environ. Sci.*, 2013, **6**, 2698–2705.
7 D.-H. Kim, R. Ghaffari, N. Lu and J. A. Rogers, *Annu. Rev. Biomed. Eng.*, 2012, **14**, 113–128.
8 C. Wang, D. Hwang, Z. Yu, K. Takei, J. Park, T. Chen, B. Ma and A. Javey, *Nat. Mater.*, 2013, **12**, 899–904.
9 S. Lee, A. Reuveny, J. Reeder, S. Lee, H. Jin, Q. Liu, T. Yokota, T. Sekitani, T. Isoyama and Y. Abe, *Nat. Nanotechnol.*, 2016, **11**, 472–478.
10 A. Chortos, J. Liu and Z. Bao, *Nat. Mater.*, 2016, **15**, 937–950.
11 Q. Liao, M. Mohr, X. Zhang, Z. Zhang, Y. Zhang and H.-J. Fecht, *Nanoscale*, 2013, **5**, 12350–12355.
12 W. Zhang, R. Zhu, V. Nguyen and R. Yang, *Sens. Actuators, A*, 2014, **205**, 164–169.
13 K. K. Kim, S. Hong, H. M. Cho, J. Lee, Y. D. Suh, J. Ham and S. H. Ko, *Nano Lett.*, 2015, **15**, 5240–5247.
14 H. Tian, Y. Shu, Y.-L. Cui, W.-T. Mi, Y. Yang, D. Xie and T.-L. Ren, *Nanoscale*, 2014, **6**, 699–705.
15 Y. Wang, L. Wang, T. Yang, X. Li, X. Zang, M. Zhu, K. Wang, D. Wu and H. Zhu, *Adv. Funct. Mater.*, 2014, **24**, 4666–4670.
16 Y. Qin, Q. Peng, Y. Ding, Z. Lin, C. Wang, Y. Li, F. Xu, J. Li, Y. Yuan and X. He, *ACS Nano*, 2015, **9**, 8933–8941.
17 K. Kanao, S. Harada, Y. Yamamoto, W. Honda, T. Arie, S. Akita and K. Takei, *RSC Adv.*, 2015, **5**, 30170–30174.
18 S. Ryu, P. Lee, J. B. Chou, R. Xu, R. Zhao, A. J. Hart and S.-G. Kim, *ACS Nano*, 2015, **9**, 5929–5936.
19 S. J. Park, J. Kim, M. Chu and M. Khine, *Adv. Mater. Technol.*, 2016, **1**, 1600053.
20 T. Lee, Y. W. Choi, G. Lee, P. V. Pikhitsa, D. Kang, S. M. Kim and M. Choi, *J. Mater. Chem. C*, 2016, **4**, 9947–9953.
21 G.-H. Lim, N.-E. Lee and B. Lim, *J. Mater. Chem. C*, 2016, **4**, 5642–5647.
22 S. Chen, Z. Lou, D. Chen, K. Jiang and G. Shen, *Adv. Mater. Technol.*, 2016, **1**, 1600136.
23 W. Wu, Y. Wei and Z. L. Wang, *Adv. Mater.*, 2010, **22**, 4711–4715.
24 R. Yu, W. Wu, Y. Ding and Z. L. Wang, *ACS Nano*, 2013, **7**, 6403–6409.
25 M. Peng, Y. Liu, A. Yu, Y. Zhang, C. Liu, J. Liu, W. Wu, K. Zhang, X. Shi and J. Kou, *ACS Nano*, 2015, **10**, 1572–1579.
26 R. Yu, W. Wu, C. Pan, Z. Wang, Y. Ding and Z. L. Wang, *Adv. Mater.*, 2015, **27**, 940–947.
27 B. Xu, D. Chen and R. C. Hayward, *Adv. Mater.*, 2014, **26**, 4381–4385.
28 D. Kang, P. V. Pikhitsa, Y. W. Choi, C. Lee, S. S. Shin, L. Piao, B. Park, K.-Y. Suh, T.-I. Kim and M. Choi, *Nature*, 2014, **516**, 222–226.
29 S. G. Yoon, H.-J. Koo and S. T. Chang, *ACS Appl. Mater. Interfaces*, 2015, **7**, 27562–27570.
30 B. Park, J. Kim, D. Kang, C. Jeong, K. S. Kim, J. U. Kim, P. J. Yoo and T. I. Kim, *Adv. Mater.*, 2016, **28**, 8130–8137.
31 Y. Tai, M. Mulle, I. A. Ventura and G. Lubineau, *Nanoscale*, 2015, **7**, 14766–14773.
32 Y. W. Choi, D. Kang, P. V. Pikhitsa, T. Lee, S. M. Kim, G. Lee, D. Tahk and M. Choi, *Sci. Rep.*, 2017, **7**, 40116.
33 T. Q. Trung and N. E. Lee, *Adv. Mater.*, 2016, **28**, 4338–4372.